https://doi.org/10.5194/egusphere-2026-2790
Preprint. Discussion started: 2 June 2026

Coupled K–Ca and Rb–Sr dating by LA-ICP-MS/MS – reaction gas optimisation and geological applications

Sarah E. Gilbert[1], Stijn Glorie[2], Jarred C. Lloyd[2]

[1]Adelaide Microscopy, Adelaide University, Adelaide, 5005, Australia

[2]Discipline of Earth Sciences, School of Physics, Chemistry and Earth Sciences, Adelaide University, Adelaide, 5005, Australia

Correspondence to: Sarah E. Gilbert (sarah.gilbert@adelaide.edu.au)

Abstract. Both the Rb-Sr and K-Ca β-decay isotopic systems can be used to date a range of mica and feldspar group minerals and have the potential to unravel cooling and alteration processes in a wide range of geological settings. The development of LA-ICP-MS/MS has enabled direct in-situ analysis of these β-decay geochronometers via chemical separation with reactive gases within the mass-spectrometer. As well as rapid analysis, the main advantage of in-situ K–Ca dating is that Ca- and Sr-bearing inclusions can be avoided, which are a limiting factor for conventional bulk mineral dating via TIMS. Both Sr and Ca are highly reactive with both SF_6 and N_2O to form M-F, M-O or M-OH reaction products, while K and Rb are unreactive with either gas, enabling efficient separation of the parent-daughter ^{40}K–^{40}Ca and ^{87}Rb–^{87}Sr isotope pairs. Additionally, mixing a small amount of H_2 with SF_6 or N_2O efficiently eliminates ^{40}Ar based interferences and reduces the background generated by the high ion load in the reaction cell when measuring mass/charge ratio (m/z) 40. This study compares the accuracy, precision and product ion sensitivity between four reaction gas combinations: SF_6 only, SF_6 plus 2 ml min^{-1} H_2, N_2O plus 7 ml min^{-1} H_2, and N_2O plus 10 ml min^{-1} H_2, by analysing a range of micas and feldspars with previously constrained dates: MDC & Kola phlogopites, Högsbo and Robins Folly muscovites, G71560 polylithionite, and F-KN and Bohus K-feldspars. Using these gas mixtures we present coupled Rb–Sr and K–Ca dates from a single ablation spot in low Ca-bearing (5–300 ppm) micas and feldspars to within 2 and 5 % age uncertainty, respectively. The direct coupling of Rb–Sr and K–Ca dates within the same ablation volume allows assessment of isotopic disturbances at high spatial resolution. The gas combination of SF_6 plus 2 ml min^{-1} H_2 was found to be most effective for coupled K–Ca and Rb–Sr dating in generating the highest sensitivity of reacted species and in reducing the background for reacted ^{40}Ca. Analysis of the FK-N feldspar from Madras, India shows the potential for the two isotopic systems to reveal decoupled dates, with the 515 ± 22 Ma Rb–Sr date representing the crystallisation of the granite and the 437 ± 38 Ma K–Ca date indicating late-stage hydrothermal activity.

1 Introduction

Laser ablation inductively coupled mass spectrometry (LA-ICP-MS) is a widely used technique for element and isotopic analyses in the earth sciences and has been used for U–Pb geochronology for over 30 years. Recent technological advancements

https://doi.org/10.5194/egusphere-2026-2790
Preprint. Discussion started: 2 June 2026

have led to the development of ICP-MS/MS systems that utilise a reaction cell between two mass selecting devices. This enables selective reactions and chemical separation of isobaric and polyatomic interferences using a range of reactive gasses. Coupling this with in-situ sampling by laser ablation has led to an expansion of applications, especially in geochronology (e.g. Gilbert et al., 2024;Gorojovsky and Alard, 2020;Olierook et al., 2020;Tillberg et al., 2020;Laureijs et al., 2021a;Rösel and Zack, 2022;Simpson et al., 2023;Glorie et al., 2023;Tamblyn et al., 2022;Brown et al., 2022). Over the past decade, this technology has been applied to the analysis of β-decay geochronometers such as Rb–Sr, K–Ca, Lu–Hf and Re–Os (Redaa et al., 2021;Simpson et al., 2021;Tamblyn et al., 2024;Hogmalm et al., 2019;Hogmalm et al., 2017;Zack and Hogmalm, 2016). In these systems the parent and daughter isotopes have the same isotopic mass, creating an isobaric interference, but can be effectively separated using a range of reaction gases: N_2O, SF_6, HN_3 or CH_4.

Radiogenic ^{40}K decays via branched pathways to ^{40}Ca (β^- decay, ~ 89%) and ^{40}Ar (electron capture, ~ 11%), enabling both K–Ca and K–Ar (^{39}Ar–^{40}Ar) dating (Nägler and Villa, 2000). These decay systems can be used to date high K, low common Ca minerals such as biotite, muscovite and K-felspars. Due to similar chemical behaviour and ionic radii, Rb readily substitutes for K in these minerals; hence, minerals that are suitable for K–Ca dating are also suitable for Rb–Sr dating. Micas are readily susceptible to deformation and alteration with reactive fluids. Thus, both isotopic systems can be reset at low temperatures through crystal deformation and dissolution/recrystallisation and have the potential to be used to determine cooling dates or to improve the understanding of low temperature diagenetic processes (Fletcher et al., 1997;Gopalan, 2008).

In the general mineral formula for micas $IM_{2\text{-}3}\square_{0\text{-}1}T_4O_{10}A_2$ (Rieder et al., 1998) Ca will substitute into the high coordination (often 12-fold) interlayer I-site along with K, Na and Rb. However, Sr has a preference for the 8-fold M-site (with Mg, Fe, Mn, Li etc) but due to its large ionic radii will often be forced in the I-site (Harrison and Lovera, 2014;Tischendorf et al., 2007;Zhao et al., 2025). While little is known about the thermal diffusivity processes of Sr and Ca in micas (Giletti, 1991;Hammouda and Cherniak, 2000; Cherniak and Dimanov, 2010), the daughter ^{87}Sr will be produced into the ^{87}Rb hosting I-site, causing a sheet charge imbalance and crystal defect meaning it will be less strongly bound in the structure compared to any common Sr sitting in the M-site. This could lead to isotopic fractionation during thermal resetting due to the differences in Sr mobility when hosted in different locations in the mineral structure. Both the common and radiogenic Ca will sit in the weakly-bonded interlayer I-site. Although closure temperatures in micas are poorly constrained, an apparent closure temperature for ^{40}Ca has been proposed at 300 °C (Harrison and Lovera, 2014), compared to 350–550 °C for the Rb-Sr system in micas (Jenkin, 1997;Nebel, 2014).

Analysis of highly precise Ca isotopes is routine via chemical dissolution and TIMS or MC-ICP-MS analysis (Farkaš, 2016;DePaolo, 2004;Antonelli and Simon, 2020), TIMS can also be used to analyse K and Ca isotopes for dating minerals (Gopalan, 2008;Heuser et al., 2002). These techniques are able to provide the highest level of analytical precision; however, the technique has some limitations: chemical dissolution and column chemistry can be time consuming and can easily incorporate common Ca-bearing inclusions within the target mineral, Ca has low ionisation efficiency by TIMS, and the precision of the $^{40}Ca/^{44}Ca$ ratios is compromised in high K/Ca minerals due to the low sensitivity of ^{44}Ca. Analysis by LA-

https://doi.org/10.5194/egusphere-2026-2790
Preprint. Discussion started: 2 June 2026

ICP-MS/MS can overcome some of these limitations via rapid analysis at high spatial resolution and is ideally suited to highly radiogenic, low Ca-bearing minerals.

In-situ Rb–Sr and K–Ca dating via LA-ICP-MS/MS was first demonstrated using N_2O and SF_6 as reaction gasses (Hogmalm et al., 2017;Zack and Hogmalm, 2016). Uptake of in-situ Rb–Sr dating via LA-ICP-MS/MS has been rapid since then (Loyola et al., 2025;Wang et al., 2022;Subarkah et al., 2022;Liebmann et al., 2022;Jegal et al., 2022;Dauphas et al., 2022;Tillberg et al., 2021;Laureijs et al., 2021b;Olierook et al., 2020;Li et al., 2020). This is primarily due to the highly efficient and 'simple' reaction chemistry of Sr with both N_2O and SF_6. However, the K–Ca analytical technique is currently underdeveloped and there are several isotopic and analytical challenges to be overcome for in-situ K–Ca dating.

The parent ^{40}K is a minor isotope of K (0.012 %), whereas the radiogenic daughter ^{40}Ca is also the most abundant common Ca isotope (96.9%). The decay constant for ^{40}K ($4.9548 \pm 0.0134 \times 10^{-10}$ per year (Renne et al., 2011)) is larger than ^{87}Rb ($1.3972 \pm 0.0045 \times 10^{-11}$ per year, (Villa et al., 2015)), resulting in a shorter half-life and faster production of the daughter ^{40}Ca than ^{87}Sr: 1.25×10^9 years (Marshall, 1998) versus 49.61×10^9 years (Villa et al., 2015). Despite the faster radiogenic ingrowth of K–Ca, the low ^{40}K parent isotopic abundance requires ~ 98,000 ug g^{-1} of K to produce ~ 4 ug g^{-1} of ^{40}Ca, compared to ~ 1000 ug g^{-1} of Rb to produce the same amount of ^{87}Sr over 1 Ga (Zack and Gilbert, 2024). Therefore, the radiogenic ingrowth of ^{40}Ca can easily be overshadowed by the presence of common Ca in the mineral of interest or as inclusions. This study aims to provide a guide for the limitations of K–Ca dating in terms of the resolvable age versus the common Ca content.

In addition, ^{40}Ar (99.6 % abundance) is also present at exceedingly high concentrations from the Ar burning ICP. It has been shown that the daughter ^{40}Ca can be efficiently separated from the non-reactive ^{40}K and ^{40}Ar using N_2O or SF_6 reaction gases (Hogmalm et al., 2017). However, the high ion load from $^{40}Ar^+$ passing through the first quadrupole into the reaction cell, has the potential to compromise the analysis and reaction mechanisms. In this study we investigate the effects of adding H_2 as a second reaction gas to mitigate the Ar^+ via charge transfer reaction ($Ar^+ + H_2 \rightarrow Ar + H_2^+$) (Eiden et al., 1996;Craig et al., 2021).

Conventional isochrons, plotting parent/stable versus daughter/stable isotopic ratios, often have high uncertainty correlations with LA-ICP-MS/MS analysis due to poor counting statistics of the lowest sensitivity stable isotopes ^{44}Ca and ^{86}Sr. Plotting 'inverse isochrons' (parent/daughter versus stable/daughter isotope ratios) generally reduces the error correlations with the least abundant stable isotope only present on one plot axis, and also improves data visualisation for highly radiogenic samples (Li and Vermeesch, 2021).

The ease of measuring multiple isotopes across the mass range is a distinct advantage for quadrupole LA-ICP-MS/MS analysis. This enables the measurement of two, or more, isotope systems simultaneously from the same ablation volume. This study investigates the accuracy of the combined measurement of both the Rb–Sr and K–Ca isotopic systems in the same ablation by LA-ICP-MS/MS in a range of micas and feldspars, and to optimise the analytical procedure via comparison of N_2O, SF_6 and H_2 reaction gases.

https://doi.org/10.5194/egusphere-2026-2790
Preprint. Discussion started: 2 June 2026

2. Sample descriptions

2.1 Mica group minerals

The MDC phlogopite was cut from a 10 x 7 x 1.5 cm crystal, sourced from the Bekily region, Madagascar (Redaa et al., 2021). It is taken to be the equivalent in geological source and age as the Mica-Mg powdered reference material distributed by the Centre de Recherches Petrographiques et Geochimiques (CRPG, (Govindaraju, 1979, 1995)). The expected age of 519.4 ± 6.5 Ma used in this study is the average reported Rb–Sr, K–Ar and U–Pb age of the region ((Hogmalm et al., 2017) and references therein). The initial $^{87}Sr/^{86}Sr$ ratio of 0.72607 ± 0.0007 was measured from two diopside analyses from the Mica-Mg phlogopite sample (Morteani et al., 2013). More recent ID-MC-ICP-MS results from the Mica-Mg powdered samples gives a relatively imprecise date of 521 ± 24 from 12 aliquots (Jegal et al., 2022) and 524.9 ± 3.6 from 1 aliquot (Redaa et al., 2022), indicating some uncertainty in the batch-to-batch reproducibility of the Rb–Sr age from the Mica-Mg powdered sample.

The Kola phlogopite was sourced from the Kovdor Massif, located on the Kola Penisnsula, Kovdorsky District, Russia. The cm-scale phlogopite book was purchased from a mineral dealer and the exact location is unknown. Similar sized phlogopites characteristic of the deposit, are formed from high temperature ultrabasic pegmatites within a carbonatite-bearing alkaline-ultrabasic complex (Amelin and Zaitsev, 2002;Krasnova, 2001). A narrow range of TIMS U-Th-Pb dates have been reported from the Kovdor Massif by Amelin & Zaitsev (2002): ca. 378 Ma (baddeleyite, discordant, lower intercept $^{206}Pb/^{238}U$), 377.52 ± 0.94 Ma (Zircon $^{208}Pb/^{232}Th$), 377.5 ± 3.5 Ma (apatite, U–Pb isochron) and 380.6 ± 2.6 Ma (apatite and calcite, U–Pb isochron). Baddeleyite dates of 377 ± 4 and 383 ± 3 have also been reported (Bayanova, 2006). Phlogopites have been dated by conventional Rb–Sr, giving a date of 378.3 ± 1.5 Ma ((Amelin and Zaitsev, 2002), recalculated using the decay constant of (Villa et al., 2015)) and initial $^{87}Sr/^{86}Sr$ of 0.70368 ± 0.00055. A weighted mean date based on U–Pb and Rb–Sr analyses of 378.1 ± 1.2 was used as the reference age in this study (Table 1).

The Robins Folly muscovite was sourced form undeformed pegmatites in the Hartz Range metaigneous province, Northern Territory, Australia, emplaced during the late stages of the Alice Springs Orogeny (450–300 Ma). The sample was collected from the same location as described in (Mortimer et al., 1987), near the Ruby Mines. (Mortimer et al., 1987) reported a whole rock Rb–Sr date of 320 ± 22 Ma (recalculated using the decay constant of (Villa et al., 2015)) with an initial $^{87}Sr/^{86}Sr$ ratio of 0.7445 ± 0.0028. Additional model muscovite and biotite dates from the same area are reported as 327–337 Ma and 329 ± 2 Ma respectively (Mortimer et al., 1987), suggesting up to 5 % age variability between samples.

The Högsbo muscovite was sampled from the Högsbo pegmatite quarry in Gothenburg, Sweden. The crystallisation age of the pegmatite, constrained by a columbite $^{207}Pb/^{206}Pb$ TIMS date of 1029.7 ± 2.0 Ma (Romer and Smeds, 1996), was used as the reference in this study, along with an initial $^{87}Sr/^{86}Sr$ ratio of 0.72000 ± 0.00010 (Hogmalm et al., 2017). In-situ Rb–Sr dates have been reported as 1037 ± 11 Ma from the Högsbo nano-powder pellet (Hogmalm et al., 2017), and 1035 ± 7 and 1039 ± 7 Ma from muscovite crystals (Rösel and Zack, 2022). More recently, an $^{40}Ar–^{39}Ar$ muscovite date of 1025.2 ± 2.2 Ma, and in-situ Rb–Sr dates between 1023 ± 2.4 Ma and 1024 ± 7 Ma have been reported in (Olierook et al., 2026). Significantly younger

https://doi.org/10.5194/egusphere-2026-2790
Preprint. Discussion started: 2 June 2026

in situ Rb–Sr dates have also been reported within the same muscovite crystals: 1003 ± 6 Ma (Rösel and Zack, 2022) and 981 ± 8 Ma (Olierook et al., 2026), suggesting some alteration of the pegmatites is recorded in the muscovite.

The G17560 polylithionite was sourced from the South Australian Museum collection from a non-specific location near Itinga, Minas Gerais, Brazil. This would place it within the Araçuaí District in the Eastern Brazilian Pegmatite Province. Similar gem-quality polylithonite specimens have been found in an artisanal mine within the Taquaral pegmatite field. Two different pegmatite suites have been identified in this region with zircon U–Pb dates of nearby granite bodies ranging from 520–480 Ma and 530–500 Ma (G5 and G4 supersuites, (Pedrosa-Soares et al., 2011)). There are no published Rb–Sr dates for these pegmatites, nor measured $^{87}Sr/^{86}Sr$ initial ratios. For this study the initial was assumed to be 0.71 ± 0.015 (assumed for enriched magmatic rocks (Rösel and Zack, 2022). The polylithionite contains very high Rb (~ 1.4 wt%) and negligible common Sr, making the Sr component highly radiogenic. Hence, the choice of initial Sr ratio has no significant effect on the calculated Rb-Sr date.

Table 1. Reference ages for minerals used in this study, with additional details in text.

Sample	Mineral	Age (Ma)	2SE (Ma)	Sr/Sr_i	~Ca_c ppm*	Reference
MDC	Phlogopite	519.4	6.5	0.72607	5-20	(Hogmalm et al., 2017;Morteani et al., 2013;Redaa et al., 2021)
Kola	Phlogopite	378	1.5	0.7037	< 5	(Amelin and Zaitsev, 2002;Bayanova, 2006)
Robins Folly	Muscovite	320	22		< 5-40	(Mortimer et al., 1987)
Högsbo	Muscovite	1029.7	2.0	0.72	< 10-50	(Hogmalm et al., 2017;Romer and Smeds, 1996)
FK-N	K-feldspar	512	30	0.7093 +/- 0.005	~ 300	(Jegal et al., 2022)
Bohus	K-feldspar	920	5	0.711 +/- 0.005	~ 300	(Eliasson and Schöberg, 1991)
G17560	Lepidolite	480–530		0.71 +/- 0.005	< 10	(Pedrosa-Soares et al., 2011)

*** Approximate common Ca concentration, this study, measured on ^{43}Ca. $^{40}Ca/^{44}Ca$ initial assumed to be 47.15 ± 0.02 (Russell et al., 1978)**

https://doi.org/10.5194/egusphere-2026-2790
Preprint. Discussion started: 2 June 2026

2.2 K-feldspars

The FK-N K-feldspar is used as an international trace element reference material, distributed by CRPG (Govindaraju, 1984), sourced from Tamil Nadu Province, India. Feldspar chips from the original source were obtained and mounted for analysis. The FK-N powdered sample has been dated by Jegal et. al (2022), giving an Rb-Sr date of 512 ± 30 Ma. Co-genetic pegmatites and leucogranites from the region have also been dated giving a Rb-Sr date of 521 ± 9 Ma and initial $^{87}Sr/^{86}Sr$ ratio of 0.7093 (Pandey et al., 1993).

The Bohus K-feldspars were separated from the Bohus granite, located in south-west Sweden. The granite massif compromises of several granitic intrusions, and has been commercially quarried since the 1840's. The granite intrudes into the Dal Group (1100 to 1050 Ma) at the end of the Sveconorwegian orogeny. It has a Rb-Sr date of 910 ± 35 Ma and an initial Sr ratio of 0.711, and K–Ar model-ages range from 861 to 680 Ma (Skiöld, 2010). A higher precision zircon U–Pb date of 920 ± 5 Ma is regarded as the crystallisation age of the Bohus granite (Eliasson and Schöberg, 1991).

3. Analytical Methods

3.1 Instrumentation

Analyses were conducted at Adelaide Microscopy, Adelaide University, using a RESOlution-LR 193 nm excimer laser system coupled to an Agilent 8900x ICP-MS/MS. The interface tubing between the laser sample chamber and the ICP torch was cleaned prior to each analytical session and was not used for the ablation of high Ca materials (e.g. NIST glasses, 8.15 wt% Ca) to minimise the potential for Ca-contamination. A pure SiO_2 glass was also ablated at the start of each session to mobilise any residual, previously ablated aerosol particles in the tubing (Gilbert et al., 2014). A Teflon bulb (~ 20 ml) was used as the signal smoothing device rather than a squid, given the latter is difficult to lean and remain Ca free. Carrier gas flow rates were 350 ml min^{-1} He, mixed with 890 ml min^{-1} Ar, and the addition of 6 ml min^{-1} N_2 to enhance sensitivity. The laser parameters for all sessions were: 3.5 J cm^{-2} fluence, 5 Hz repetition rate, and 100 µm spot size. All instrument parameters, including ICP-MS/MS lens tuning are provided in Table S1.

A range of reaction gas mixtures and flow rates were tested based on the previously published reaction products of Sr and Ca (Hogmalm et al., 2017;Redaa et al., 2021). The aim was to determine the optimal gas flow rates in terms of reaction product ion sensitivity, and the signal to background ratio for ^{40+X}Ca (where X represents the mass shift of the product ions, see reaction gas optimisation section below). The four gas combinations selected for detailed testing were: SF_6 only (0.77 ml min^{-1}, 40%), SF_6 and H_2 mix (0.57 ml min^{-1}, 30% and 2 ml min^{-1}, respectively), and N_2O and H_2 mixed in two different proportions: 0.16 ml min^{-1} N_2O, 15% and 7 ml min^{-1} H_2; and 0.16 ml min^{-1} N_2O, 15% and 10 ml min^{-1} H_2. These setting are referred to as SF_6 only, SF_6 + H_2, N_2O + low H_2 and N_2O + high H_2, from here on. Reaction gas combination of N_2O without H_2 was not tested in detail due to the significant production of $^{40}Ar^{16}O$ interference. When H_2 is added, Ar is neutralised via a charge transfer reaction (Eiden et al., 1996). In our experiments, no Ar reaction products were detected (measured as ^{36+X}Ar), indicating the

https://doi.org/10.5194/egusphere-2026-2790
Preprint. Discussion started: 2 June 2026

charge transfer reaction is thermodynamically favourable in the reaction cell. Both SF_6 and N_2O gases were introduced into the reaction cell using the third mass flow controller (MFC3), N_2O as 99.999 % purity, and SF_6 as a mixture of 10% SF_6 in He (referred to as SF_6 throughout). The 99.999% purity H_2 was introduced via a separate, dedicated MFC.

3.2 Reaction products

To determine the most abundant rection products for Ca and Sr, product ion scans (PIS) were conducted. The first quadrupole (Q1) was set to a mass-to-charge ratio (m/z) of 44 or 88, respectively, and Q2 scanned across the mass range with mass shifts of 0 to 150 amu. When using SF_6, both with and without the addition of H_2, the predominant reaction products were CaF and SrF (+19 amu mass shift; Fig. 1a). For reactions with N_2O plus H_2, hydroxide (OH) product ions were most abundant (+17 amu mass shift; Fig. 1b). Thus, based on the PIS results, the highest abundant reaction products of $Ca^{19}F$, $Sr^{19}F$, $Ca^{17}OH$ and $Sr^{17}OH$ were used in further analysis. For both Ca and Sr, measurable amounts of hydrides and oxides were also present. For Ca, heavier $Ca(H_2O)OH$ and $Ca(H_2O)F$ were also detected. These H_2O bearing reaction products may have be caused by a contaminant (e.g. air or moisture) in the H_2 gas lines, as these occurred without the deliberate addition of oxygen i.e. with SF_6. Additional gas line flushing is recommended to reduce the production of these molecules.

For SF_6 the PIS also showed the SF_x breakdown products at masses 51, 70, 89, 108 and 127 amu (Fig. 1). These reaction products occur across 3 masses in each experiment, reflecting the isotopic proportions of S. As these product ions are created within the reaction cell from the breakdown of the SF_6 reaction gas itself, their occurrence is independent of the ions that passes through Q1 into the reaction cell. For example, the SF_6 reaction products were also measurable at the same rates when Q1 was set to 3 amu, meaning no ions were entering the reaction cell. For K-Ca and Rb-Sr isotopic analysis these products do not affect the measurements, however they can have implications for the range of trace elements monitored in the same analysis; e.g. ^{51}V, ^{53}Cr, ^{89}Y, and ^{90}Zr will all have elevated backgrounds when SF_6 is used as reaction gas.

The isotopes measured with dwell times (ms) in brackets, were: ^{27}Al (5), ^{36+X}Ar (20), ^{39}K (10), ^{39+X}K (20), ^{40+X}Ca (50), ^{42+X}Ca (50), ^{43+X}Ca (50), ^{44+X}Ca (100), ^{85}Rb (20), ^{86+X}Sr (50), and ^{87+X}Sr (50). For the reacted isotopes X represents a mass shift of either 19 (e.g. $^{40}Ca^{19}F$) when using SF_6 reaction gas and 17 (e.g. $^{40}Ca^{17}OH$) when using the N_2O and H_2 mixture. The presence of unreacted ^{40}Ca and ^{87}Sr prevents the direct measurement of the parent isotopes, so ^{39}K and ^{85}Rb were measured as proxies for ^{40}K and ^{87}Rb respectively and calculated assuming natural isotopic abundance (Hogmalm et al., 2017;Redaa et al., 2021).

https://doi.org/10.5194/egusphere-2026-2790
Preprint. Discussion started: 2 June 2026

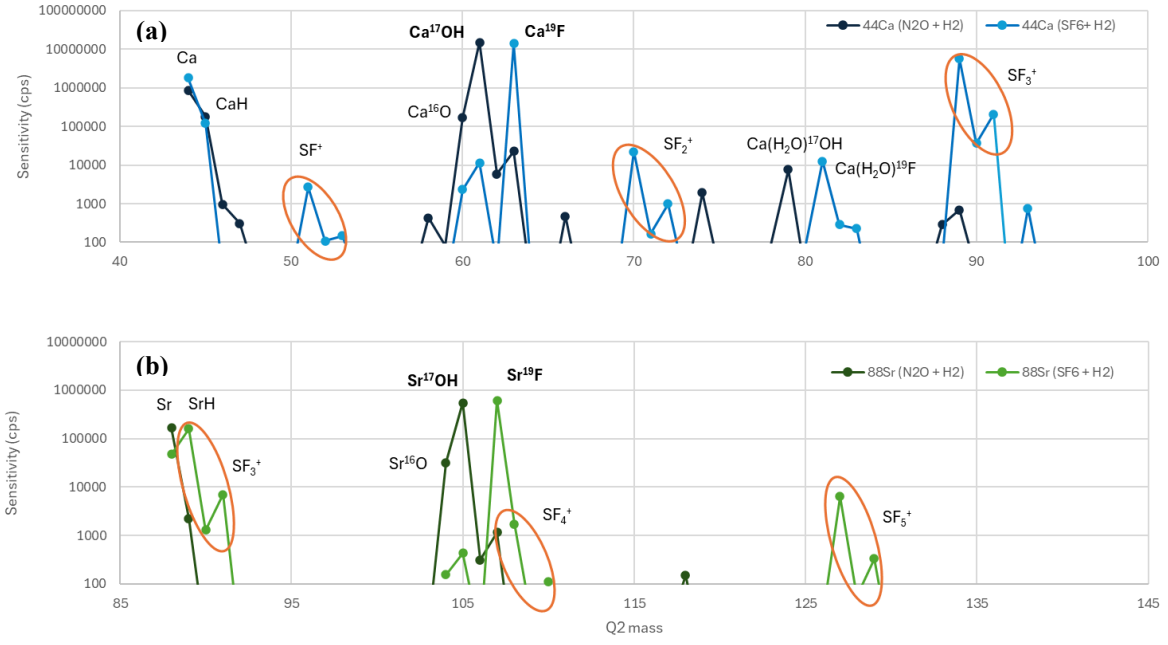

Figure 1. Product ion scans for ^{44}Ca (a) and ^{88}Sr (b) using $SF_6 + H_2$ and $N_2O + H_2$ reaction gases, measured on NIST SRM 610 glass and plotted to show reaction products greater than 100 cps only. Major reaction product ions that were chosen for Sr and Ca analysis in further experiments are highlighted in bold. Circled in orange are the SF_6 gas breakdown products (SF_x).

3.3 Analysis of mass 40 and reaction gas optimisation

Measurement of ^{40}Ca, the major Ca isotope (96.9% abundance), is complicated by the presence of the major isotope of Ar (99.6% abundance), as well as the parent ^{40}K. Since $^{40}Ar^+$ is the most abundant ion produced in the Ar burning ICP, the total number of ions passing through Q1 (set at 40 amu) and entering the reaction cell is very large, greater than the maximum detectable 8 x 10^{10} cps. The total ion load is thus likely to significantly exceed the maximum capacity of the reaction cell in terms of ensuring efficient and controlled reactions.

Product ion scans were recorded at m/z 40, both in the gas background (^{40}Ar) and while ablating NIST SRM 610 glass (^{40}Ar and ^{40}Ca). Figure 2 illustrates the additional complexity of measuring ^{40}Ca compared to the measurement of ^{44}Ca. There are four major observations of note. Firstly, the enhancement of the reaction gas breakdown product ions e.g. 10^6 cps for SF^+ when Q1 = 40 (Fig. 2), compared to 2000 cps at Q1 = 44 (Fig. 1a).

Secondly, the detection of N_2O product ions, such as N_2O-N_2O^+ and N_2OH-N_2O^+ on m/z 62 and 63, which were not detected at other Q1 masses (Fig. 1). This is likely due to the high density of Ar^+, reacting with and breaking down the reaction gasses. Thirdly, N_2O and SF_6 can attenuate the Ar^+ ions via charge transfer reactions, although not as effectively as the addition of H_2. The on-mass 40 amu measurement is still significant for reactions without H_2 (c. 10^6 cps with SF_6 and c. 10^8 cps with N_2O; Fig. 2), however, this is lower compared to when no reaction gasses are used (above the maximum 8 x 10^{10} cps). As predicted,

https://doi.org/10.5194/egusphere-2026-2790
Preprint. Discussion started: 2 June 2026

the addition of H_2 to both SF_6 and N_2O reduced the detectable 40 amu to < 1000 cps. Fourthly, a high gas background was observed on all Q2 masses when Q1 was set to 40 amu, indicated with the dashed line in Figure 2. The addition of H_2 to SF_6 has little effect on this background (red and orange lines Fig. 2), whereas the addition of H_2 to N_2O significantly reduced the background (light and dark blue lines Fig. 2). Therefore, this effect is likely to be caused by the presence of Ar^+ ions, as opposed to the reactive H^+ ions generated from the Ar-H_2 charge transfer reaction. This background can be significant at the CaF and CaOH reaction product masses, 57 and 59 amu (highest values > 10^4 cps in the example below), and subsequent testing detailed below aimed to optimise the reaction gas flow rates to minimise this background. Ultimately, sensitivity is a function of signal to background ratio, thus background signals need to be carefully monitored prior to analysis.

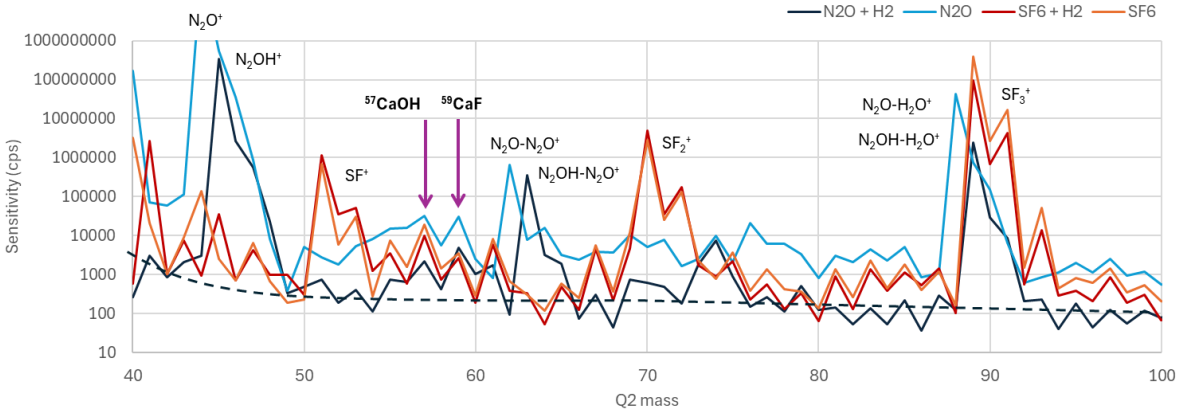

Figure 2. Gas background product ion scans (no sample ablation) with Q1 = 40 amu using four different reaction gas mixtures: N_2O only (light blue), N_2O + H_2 (dark blue), SF_6 only (orange) and SF_6 + H_2 (red). The labelled high cps peaks represent the breakdown of the reaction gases themselves, and where Ca reaction products of interest would be measured at m/z 57 and 59.

The reaction gas flow rates and proportions between the gases (SF_6, N_2O and H_2) were systematically varied to determine their effect on $^{40+X}$Ca reaction products. Count rates on m/z = 57 (Q1 = 40, Q2 = 57) and 59 (Q1 = 40, Q2 = 59) were measured, in the gas background and when ablating NIST610 to produce CaOH and CaF reaction products. The signal to background ratios were compared to determine the optimal flow rates for each reaction gas (Fig. 3).

As the SF_6 flow rate was increased from an initial rate of 20% (0.38 ml min^{-1}), the sensitivity of CaF increased to a plateau at 30% for SF_6 + H_2 (0.57 ml min^{-1} SF_6, 2 ml min^{-1} H_2) and 40% for SF_6 only (0.77 ml min^{-1}), while the background decreased slightly or was stable (Fig. 3). These sensitivity plateaus occur at the flow rates that give the maximum reaction efficiency. Higher gas flow rates eventually attenuate the signal due to increased collisions in the cell. While the addition of SF_6 only can resolve the Ar interference on ^{40}Ca (no ^{40}ArF reaction), the SF_6 + H_2 mixture results in slightly higher sensitivity for $^{40}Ca^{19}F$ and, more importantly, a significantly lower background (signal to background ratio increases from 3650 to 5770, Fig. 3).

Signal and background data was collected for a range of N_2O flow rates, from 0.16 to 0.32 ml min^{-1} (15–30%) using 7 ml min^{-1} H_2 (Fig. 4a). The sensitivity dropped with increasing N_2O flow rate, lowering of the signal to background ratio. The same relationship was observed when using higher H_2 flow rates (e.g. 10 ml min^{-1}). Figure 4b presents cps data using 0.16 ml min^{-1} N_2O (15%) and varying the H_2 flow from 5–10 ml min^{-1} (with 10 ml min^{-1} being the highest flow rate achievable on the mass-

https://doi.org/10.5194/egusphere-2026-2790
Preprint. Discussion started: 2 June 2026

flow controller). Signal sensitivity and background both decreased with increasing H_2 gas flow, however, the highest signal to background ratio was achieved using a maximum of 10 ml min^{-1} H_2. The higher H_2 gas flow rates not only effect the ^{40}Ca sensitivity, but they also effect the sensitivity of the minor ^{44}Ca, where higher sensitivity is beneficial to improve overall uncertainty of the measured ratios. These two conditions of 0.16 ml min^{-1} N_2O and 7 ml min^{-1} H_2 (N_2O + low H_2), and 0.16 ml min^{-1} N_2O and 10 ml min^{-1} H_2 (N_2O + high H_2) were used for further testing of mineral samples. The 7 ml min^{-1} H_2 flow rate is a compromise in signal to background ratios, while maintaining higher signal sensitivity.

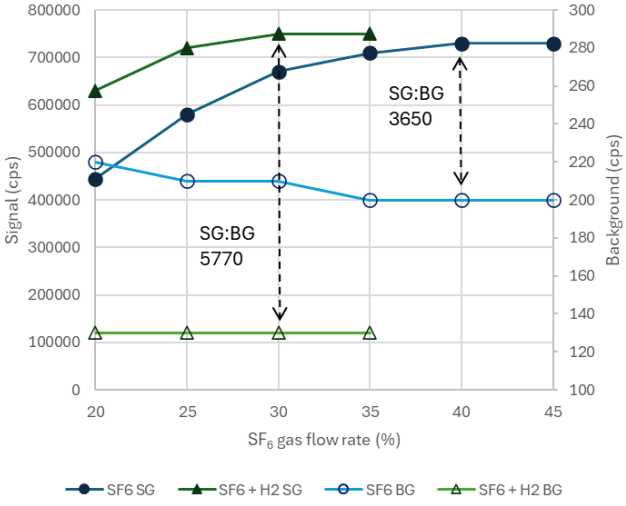

Figure 3. Signal (SG) and background (BG) cps at m/z 59 (CaF) for the optimisation of SF_6 gas flow rate. Units in % of total flow of the mass flow controller, where 30% is a flow of 0.57 ml min^{-1} and 40% is 0.77 ml min^{-1}. Experiment 1 (blue symbols) is SF_6 gas only and experiment 2 (green symbols) is SF_6 with 2 ml min^{-1} H_2.

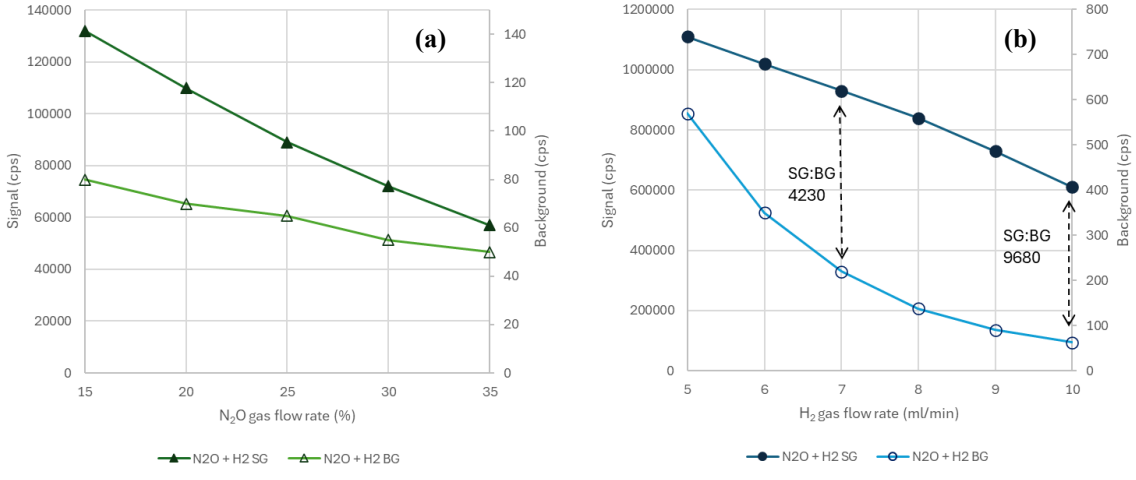

https://doi.org/10.5194/egusphere-2026-2790
Preprint. Discussion started: 2 June 2026

Figure 4. Signal (SG) and background (BG) cps at m/z 57 (CaOH) for the optimisation of N_2O and H_2 gas flow rates. (a) Using 15% N_2O (0.16 ml min^{-1}) and varying the H_2 flow from 5-10 ml min^{-1}. (b) Using 7 ml min^{-1} H_2 and varying the N_2O flow from 15-30% (0.16 to 0.32 ml min^{-1}).

3.4 Calibration strategies

Isotopic ratios were calibrated using a glass reference material, manufactured at the Institute for Photonics and Advanced Sensing, Adelaide University. The glasses were made from major components of SiO_2-Na_2O-(BaO)-MgO, doped with known quantities of K, Ca, Sr and Rb (referred to as SNBM-1 and SNM-1). The raw materials were ball-milled for 1 hour to achieve thorough mixing and then loaded into a platinum crucible. The batch materials were melted at 1500 °C for 2 hours and cast into a brass mould. On the following day, the sample was annealed at 520 °C for 2 hours to relieve internal stress. To improve the homogeneity of the glass, the initial glass was powdered and re-melted at 1500 °C for 2 hours, followed by the same casting and annealing steps as before.

The synthetic glasses were used in preference to the more commonly used, high-Ca glasses: NIST SRM 610 (8.15 wt% Ca) and BCR-2G (5.05 wt% Ca), to avoid Ca contamination from remobilisation of previously ablated material in the interface tubing (i.e. false signal). The manufactured glasses also enabled customisation of the K, Rb, Sr and Ca concentrations to match the electron multiplier detector modes (pulse or analog counting) between reference materials and samples.

Initial testing used the SNBM-01 glass with a SiO_2-Na_2O-BaO-MgO matrix doped with 2000 ppm K and Rb, and 500 ppm Ca and Sr. However, ablating this glass with our standard 100µm / 5Hz laser settings resulted in ^{40}Ca being measured in analog mode, while the samples were all in pulse mode. Note that ^{44}Ca is always measured in pulse mode, given the natural abundance ratio between ^{44}Ca and ^{40}Ca is c. 47. Reducing the laser beam size or repetition rate to lower ^{40}Ca signal into pulse mode caused an unfavourable reduction in precision for the mineral samples. The MDC phlogopite (519 ± 6.5 Ma, $^{87}Sr/^{86}Sr_i$ 0.72607 (Hogmalm et al., 2017;Morteani et al., 2013;Redaa et al., 2021) was used as the mineral-matched reference material to correct for matrix-dependent mass bias on $^{87}Rb/^{87}Sr$ and $^{40}K/^{40}Ca$, where the ^{40}Ca signal was collected in pulse mode, compared to analog in the SNBM-1 glass. As all other samples were also in pulse mode, correcting the $^{40}K/^{40}Ca$ ratios to MDC also incorporated a pulse-analog component to the correction. This two-step correction follows the method outlined in (Glorie et al., 2024a). The Kola phlogopite was used to calculate a P-A correction for ^{40}Ca using the offset between the calculated, unanchored $^{44}Ca/^{40}Ca$ intercept and the expected ratio of 47.15 ± 0.02 (Russell et al., 1978). Kola was used in preference to MDC for the P-A correction for $^{44}Ca/^{40}Ca$ as it produced higher variability in $^{44}Ca/^{40}Ca$ ratios between analyses, leading to more robust isochron regression and calculated initial $^{44}Ca/^{40}Ca$ ratio. The P-A correction was robust enough for comparative testing to optimise the reaction gas flows, however, it is not recommended as a routine protocol due to differences in mass-bias drift between pulse and analog modes (Glorie et al., 2024b).

A second glass, SNM-01, was made with a SiO_2 -Na_2O-MgO matrix and doped with 2000 ppm K, 1000 ppm Rb, 100 ppm Ca and 500 ppm Sr. These concentrations were chosen such that ^{39}K and ^{85}Rb were measured in analog detector mode and ^{40+X}Ca and ^{87+X}Sr were measured in pulse mode at 100 µm spot size. This better matched the detector mode in the samples to avoid

https://doi.org/10.5194/egusphere-2026-2790
Preprint. Discussion started: 2 June 2026

the need for pulse-analog correction. The reference values used for normalisation of the measured isotopic ratios for both glasses were calculated from the nominal concentrations, assuming natural isotopic abundances and molar proportions.

The synthetic glasses were used to correct for instrument drift, down-hole fractionation and matrix independent mass-bias using the LADR data processing software (Norris and Danyushevsky, 2018). The correction to the matrix matched age reference material (MDC) was calculated in Excel. All uncertainties are reported at the 95% confidence interval. The individual measurement uncertainties include the excess scatter of the ratios measured in the glass reference material as calculated in LADR. The MDC age correction factor was applied to the measured $^{87}Rb/^{87}Sr$ and $^{40}K/^{40}Ca$ ratios, and the calculated MDC age uncertainty (typically ~ 2 % for K-Ca and ~ 1 % for Rb-Sr) was propagated onto the uncertainty of the sample isochron dates. The long-term reproducibility of Rb-Sr dates at the Adelaide Microscopy isotope facility is ~1.5%, which is similar to 1.6 % reported in (Olierook et al., 2026), and 1.4% in (Rösel and Zack, 2022). This additional uncertainty was propagated onto the final dates: 1.5% for Rb-Sr and a more conservative 2% for K-Ca as a realistic estimate, in the absence of long-term data. SNB-01 was used as the primary refence material for $^{44}Ca/^{40}Ca$ and $^{86}Sr/^{87}Sr$ ratios without further correction, as isotopic ratios of the same element are not subject to matrix-dependent fractionation (Redaa et al., 2021;Gorojovsky and Alard, 2020). The $^{87}Sr/^{86}Sr$ initial ratios used for plotting isochrons were either obtained from the literature when known (Table 1) or an assumed value based on the recommendations by (Rösel and Zack, 2022). A $^{40}Ca/^{44}Ca$ initial value of 47.15 ± 0.02 was used for al K-Ca isochrons, as the range of naturally occurring Ca isotopic ratios can be considered invariant within the uncertainty of the LA-ICP-MS/MS measurements (Russell et al., 1978). This is a significant benefit of the K-Ca method, which allows direct calculation of dates for every analysis without a need to assume initial ratios.

4 Results & Discussion

4.1 Down Hole Fractionation

Both Rb/Sr and K/Ca isotope ratio pairs have contrasting element volatilities with Rb and K being the more volatile (Jackson, 2008). Hence down-hole fractionation (DHF) between the elements during ablation is likely and has been described elsewhere for Rb-Sr (Gorojovsky and Alard, 2020;Redaa et al., 2021;Glorie et al., 2024a). The DHF effects were minimised in this study by using a relatively large laser spot size (100 µm) and 5 Hz repetition rate to reduce the depth to diameter ratio of the crater. Nevertheless, DHF was still observed for both isotope pairs (Fig 5).

For Rb/Sr there is very little difference in DHF between the materials after the first 10s of ablation, with the exception of Bohus feldspar which shows a more variable average signal curve during the ablation (Fig 5a, Table S9) (Lloyd et al., 2024). The relative differences between materials are more pronounced for K/Ca ratios, especially during the first 10 s of ablation (Fig 5b), with up to 10% DHF, compared to 5% for Rb/Sr. The SNM glass, MDC, G17560 and Kola micas all have relatively flat K/Ca ratios which is likely to be representative of laser induced DHF. The more variable profiles are primarily due to variation in common Ca, rather than an ablation effect. This was most pronounced for feldspar, where the fewest number of signals were averaged due to naturally heterogeneous common Ca within the ablation volume of the feldspars, producing more

https://doi.org/10.5194/egusphere-2026-2790
Preprint. Discussion started: 2 June 2026

325 variable average K/Ca. The main outlier is Högsbo, for which the steeper curve is attributed to minor common Ca contamination on the surface, which potentially penetrated along cleaves into the subsurface. Despite 7 shots pre-ablation, the common Ca signal was predominantly higher at the start of the signals before decaying to a stable level. When pre-ablation shots were recorded, the Ca signal was significantly higher than during the main ablation, compared to major elements which had similar sensitivity, indicating surface contamination of Ca. For both causes of variable common Ca, the most stable part
330 of the signal was selected to calculate dates, although the whole signals are used to generate the ratio curves in Figure 5. Typically, the first 10 s of ablation was not included in the signal selection to minimise DHF differences between matrices.

The SNM-01 glass was used to correct for DHF in the other materials. The average curve for SNM-01 is slightly flatter compared to the micas (Fig. 5), which is likely to under-correct the minerals. However, no residual slope was observed on individual analysis ratios for the minerals within the noise of the signals, and any residual bias is assumed to be corrected as a
335 component of the matrix-match mineral age correction (to MDC phlogopite). In the current absence of data processing software which can use isochronous mineral-matched reference materials to correct DHF directly, the assumption that SNM-01 is a suitable material for DHF correction is tested with the calculated mineral dates presented below. Matrix effects may become apparent at smaller spot sizes due to increased differences in DHF curves between matrices, and as the technique improves and signal uncertainties are reduced.

340

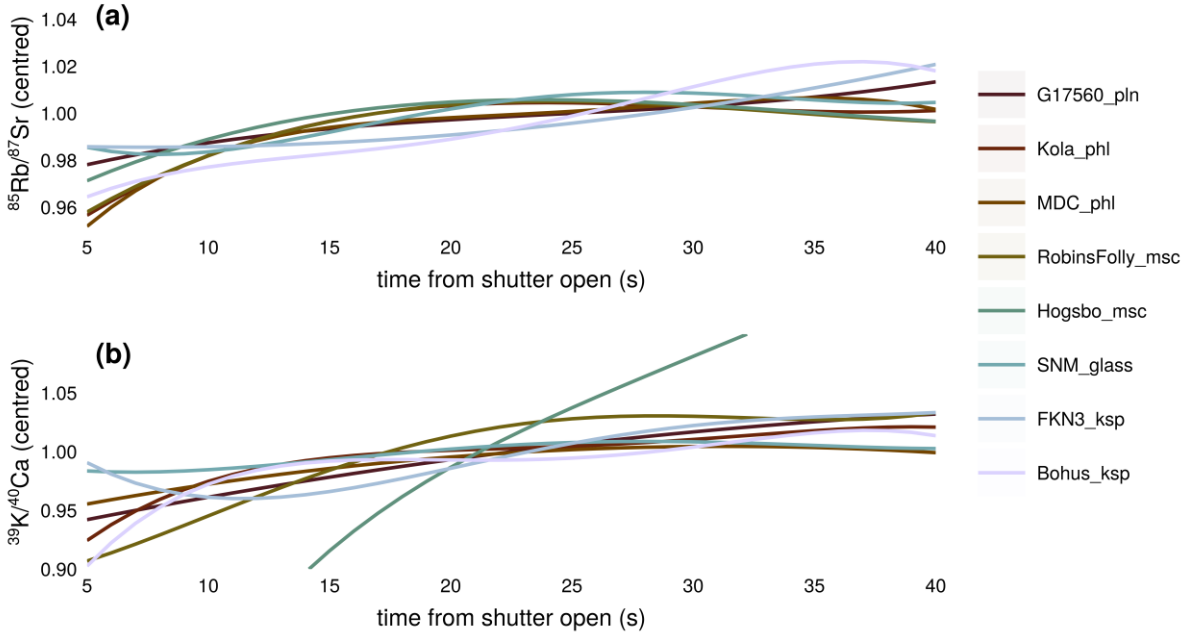

Figure 5. Down hole fractionation curves for (a) $^{85}Rb/^{87}Sr$ and (b) $^{39}K/^{40}Ca$ ratios in the SNM-1 glass, micas and feldspars, starting 5 seconds after the start of ablation (signal has stabilised by this time). Each line represents an average of between 10-30 individual
345 **signals, excluding those displaying the most variable common Ca signals. Contributing individual signals are centred to a value of 1.0 so that the effects of mass bias and drift are removed as per Lloyd et al. (2025). Note the y-axis scales in (a) and (b) are different to exaggerate the curves to aid visual interpretation.**

https://doi.org/10.5194/egusphere-2026-2790
Preprint. Discussion started: 2 June 2026

4.2 K–Ca and Rb–Sr dates of micas and feldspar

4.2.1 Reaction gas optimisation – micas

The MDC phlogopite was used as the matrix-matched reference material for all other samples analysed. Typical isochrons are shown in Figure 6 for K-Ca and Rb-Sr (see Appendices 3a-f for isochrons for all gas mixtures). There was a much larger spread in $^{44}Ca/^{40}Ca$ ratios compared to $^{86}Sr/^{87}Sr$, despite the data points being collected from the same ablations. This was observed in most of the minerals analysed. It suggests the natural variation in the minor common ^{44}Ca and ^{86}Sr are poorly correlated in phlogopite further suggesting that they can substitute differently into the mica structure (I- versus M-sites), in contrast to Rb which readily substitutes for K in the I-site. The MDC signals with the highest $^{44}Ca/^{40}Ca$ ratios had stable signals throughout the ablation, indicating ^{44}Ca is incorporated within the mineral structure, rather than being a product from Ca-bearing mineral micro-inclusions. If Ca and Sr can be hosted differently, this supports the theory that Ca and Sr can diffuse and be reset under different conditions, leading to potential de-coupling between the Rb–Sr and K–Ca apparent dates (Fletcher et al., 1997).

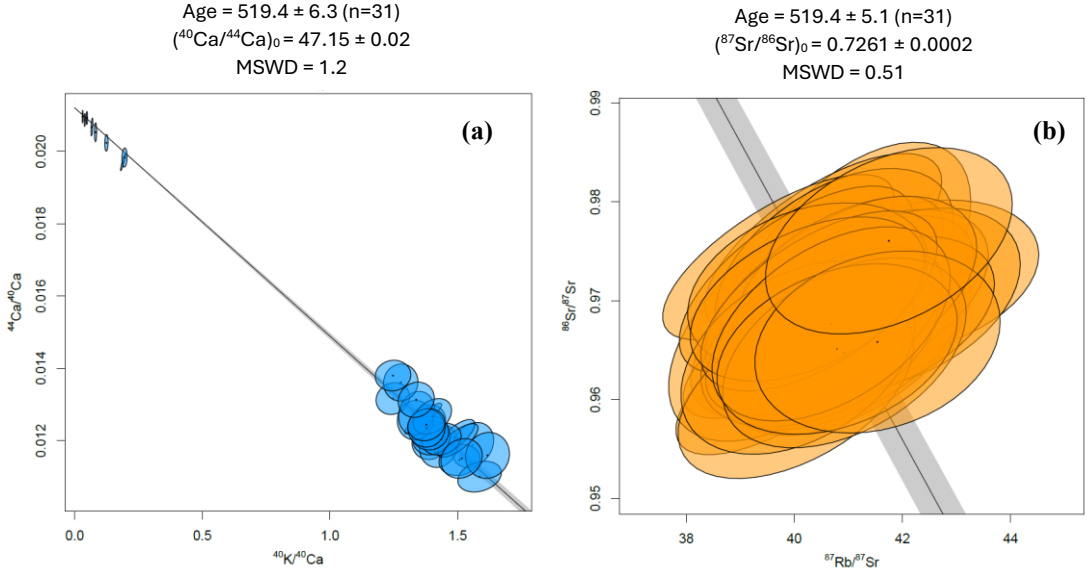

Figure 6. Representative K-Ca (a) and Rb-Sr (b) isochrons for MDC using SF_6 + H_2 reaction gasses. Dates are matrix-offset corrected to MDC itself; thus, they are equivalent to the reference age. Date uncertainties are analytical only, and this was propagated onto the date uncertainties of the other samples.

Robins Folly biotite and Högsbo muscovite give accurate dates within uncertainty for both Rb–Sr and K–Ca using three different reaction gas mixtures (Fig 7, Table S2). The exception is N_2O + high H_2, which gave a K–Ca date for Robins Folly

https://doi.org/10.5194/egusphere-2026-2790
Preprint. Discussion started: 2 June 2026

that is > 5% too old. The agreement between the K–Ca and Rb–Sr dates for these micas demonstrates that phlogopite (MDC) is a suitable matrix matched reference material for muscovite, within the uncertainty of the technique. It further demonstrates that the choice of reaction gas, SF_6 or N_2O, has little effect on the accuracy. The least consistency between isotope systems was obtained when using a N_2O + high H_2 flow. The highest sensitivity and highest signal to background ratio was achieved for reacted ^{40}Ca with SF_6 + H_2 (Fig 3, Fig 8). The highest Sr sensitivity was achieved using either SF_6 + H_2 and N_2O + low H_2. Using SF_6 only, or too high H_2 flow rate with N_2O, results in significantly lower sensitivity. The enhanced sensitivity with SF_6 + H_2 is considered advantageous for producing the best theoretical precision of individual isotope ratio measurements due to improved counting statistics on the lowest abundance isotope ^{44}Ca.

https://doi.org/10.5194/egusphere-2026-2790
Preprint. Discussion started: 2 June 2026

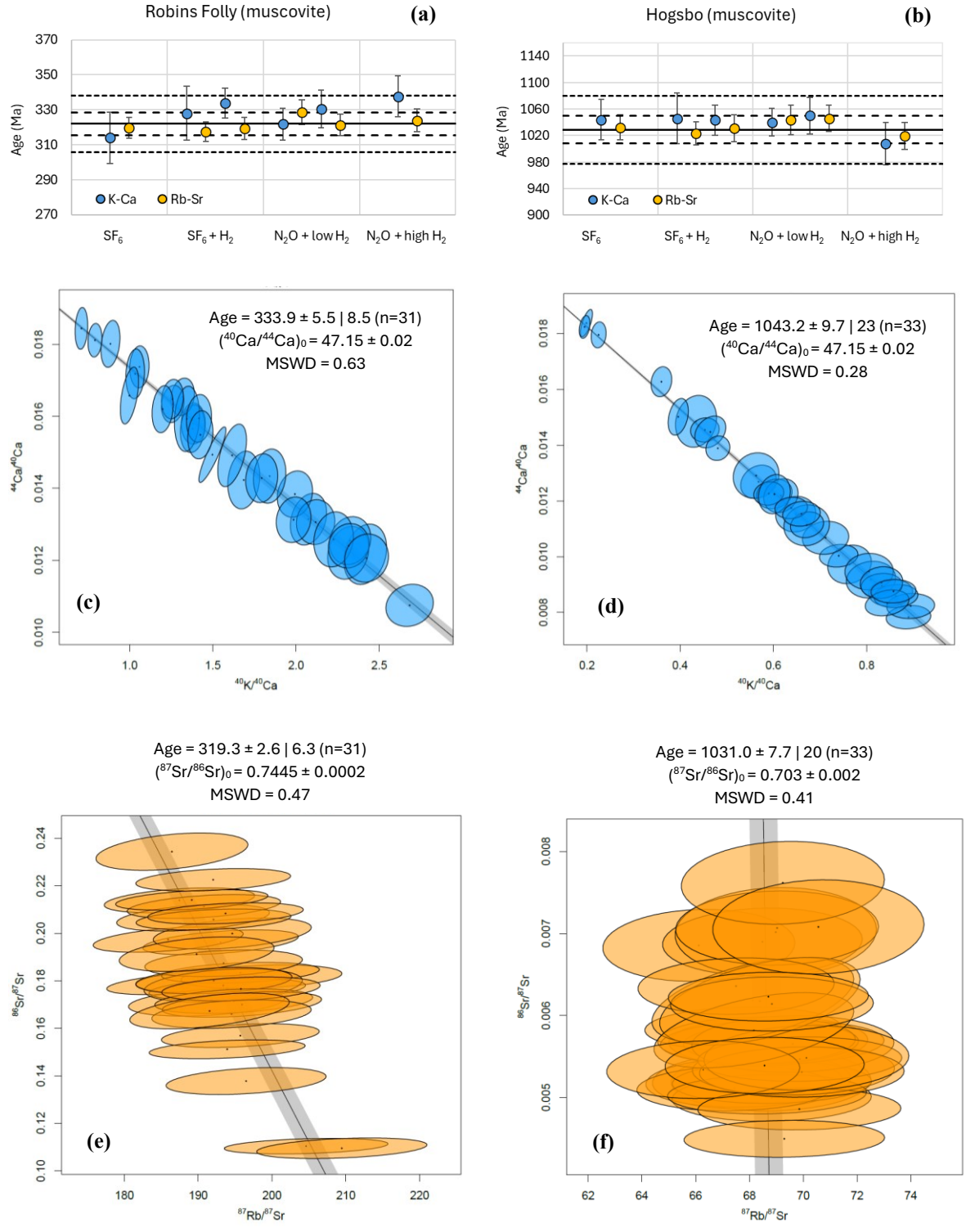

https://doi.org/10.5194/egusphere-2026-2790
Preprint. Discussion started: 2 June 2026

Figure 7. (a and b) Comparison in calculated K-Ca and Rb-Sr dates between the four reaction gas experiments for Robins Folly and Högsbo muscovites. Uncertainty bars represent 2SE propagated uncertainties. The solid horizontal line represents expected age, long and short dashed horizontal lines are ± 2 and 5% of expected age, respectively. Indicative K–Ca (c & d) and Rb–Sr (e & f) isochrons using SF_6 + H_2 reaction gas, with matrix matched age correction to MDC phlogopite. Analytical and total systematic age uncertainties are both reported with the isochrons (x | y).

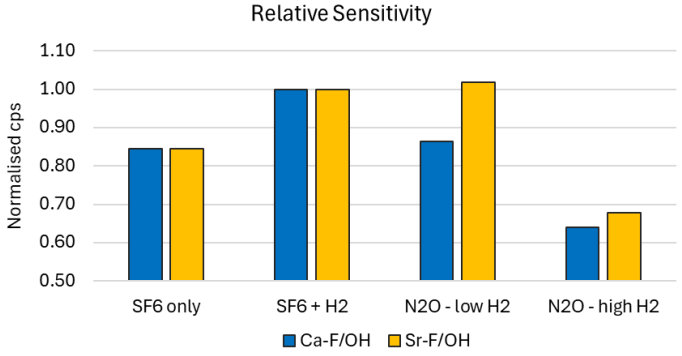

Figure 8. Sensitivity of $^{40}Ca^{19}F$ or $^{40}Ca^{17}OH$, and $^{88}Sr^{19}F$ or $^{88}Sr\ ^{17}OH$, measured on SNMB-1 glass, plotted relative to the SF_6 + H_2 reaction gas mixture.

The Rb–Sr dates for Kola are slightly older than expected, but within 3% when using SF_6 with or without H_2 (Fig 9a). However, the K-Ca ages for Kola, corrected to MDC, are highly variable with poor reproducibility between repeat sessions with both SF_6 and N_2O reaction gases, and apparent dates tending up to ca. 6% older than Rb-Sr dates (Fig 9a). Likewise, G17560 K-Ca dates also show poor reproducibility (Fig 10a), but with almost identical relative offsets as Kola. When G17560 is corrected against Kola, rather than MDC (Fig 10b), the measured K-Ca dates are consistent within uncertainty for all reaction gas combinations tested, and K-Ca dates are slightly younger than the Rb-Sr dates. These two micas have the lowest common Ca of the micas analysed (< 5 ppm), suggesting a potential bias or interference effecting the low abundance ^{44}Ca. Increasing the dwell time further for ^{44}Ca for future analyses may help to improve counting statistics and bias at low levels. This suggest that matching the Ca concentration between the matrix matched correction material and the samples is important for low Ca micas.

https://doi.org/10.5194/egusphere-2026-2790
Preprint. Discussion started: 2 June 2026

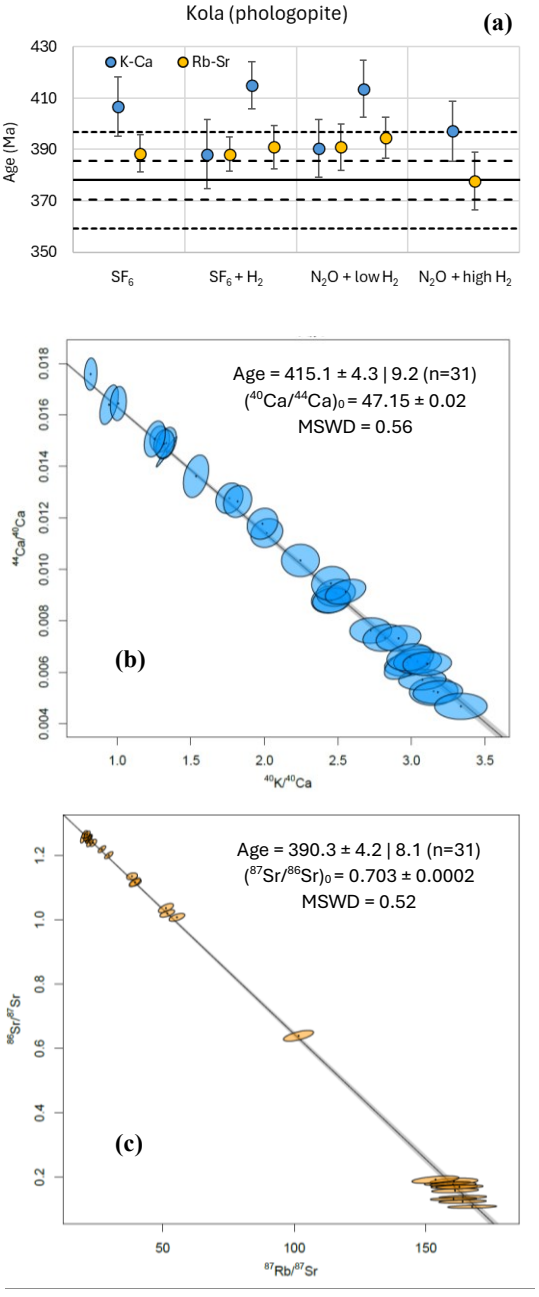

Figure 9. (a) Comparison in calculated K–Ca and Rb–Sr dates between the four reaction gas experiments for Kola phlogopite. Uncertainty bars represent 2SE propagated uncertainties. Solid horizontal line represents expected age, long and short dashed horizontal lines are ± 2 and 5% of expected age, respectively. Indicative K–Ca (b) and Rb–Sr (c) isochrons using $SF_6 + H_2$ reaction gas, with matrix matched age correction to MDC phlogopite. Analytical and total systematic age uncertainties are reported with the isochrons (x | y).

https://doi.org/10.5194/egusphere-2026-2790
Preprint. Discussion started: 2 June 2026

405

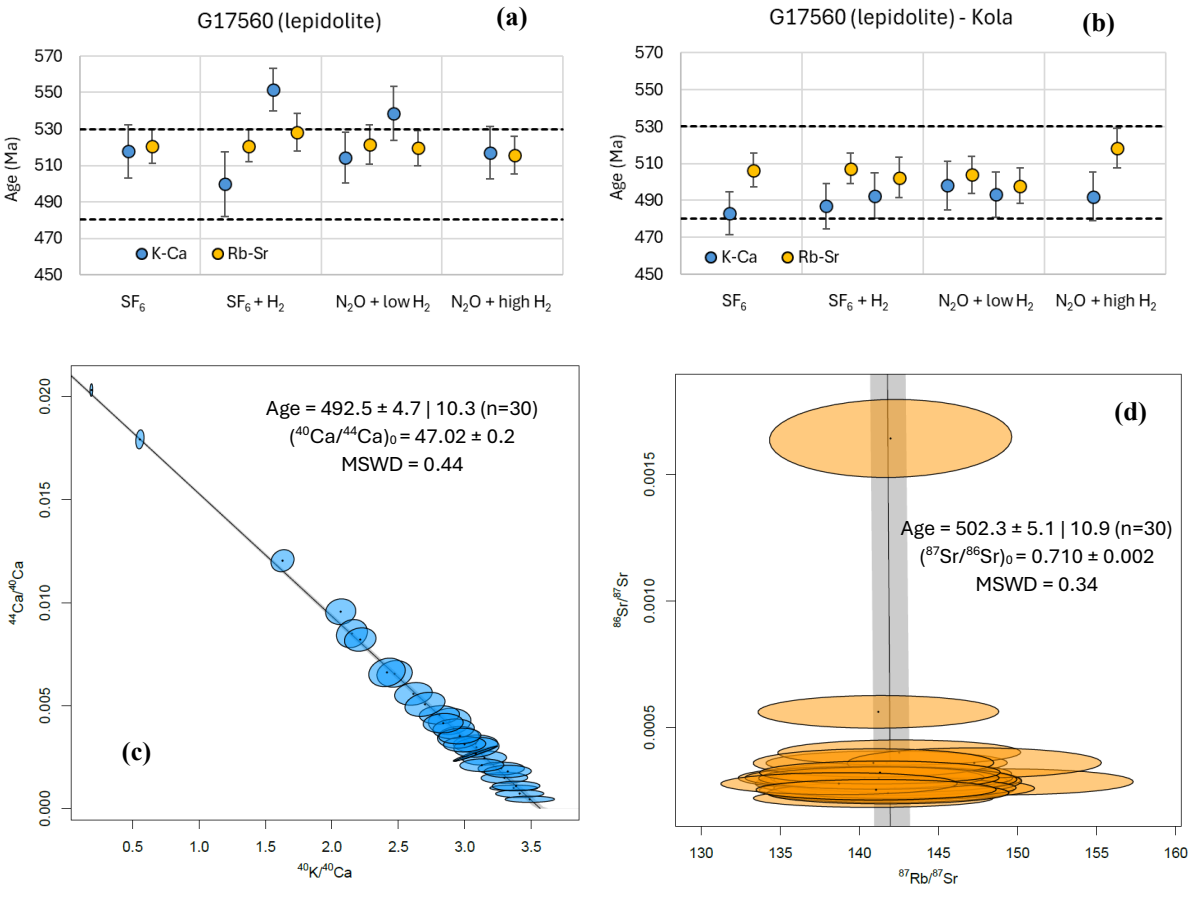

Figure 10. (a & b) Comparison in calculated K–Ca and Rb–Sr dates between the four reaction gas experiments for G17560 polylithionite normalised to MDC (a) and Kola (b). Uncertainty bars represent 2SE propagated uncertainties. Dashed horizontal 410 **lines indicate the expected age range from the region. Indicative K–Ca (c) and Rb–Sr (d) isochrons using SF_6 + H_2 reaction gas, with matrix matched age correction to Kola phlogopite. Analytical and total systematic age uncertainties are reported with the isochrons (x | y).**

https://doi.org/10.5194/egusphere-2026-2790
Preprint. Discussion started: 2 June 2026

4.2.2 Feldspars

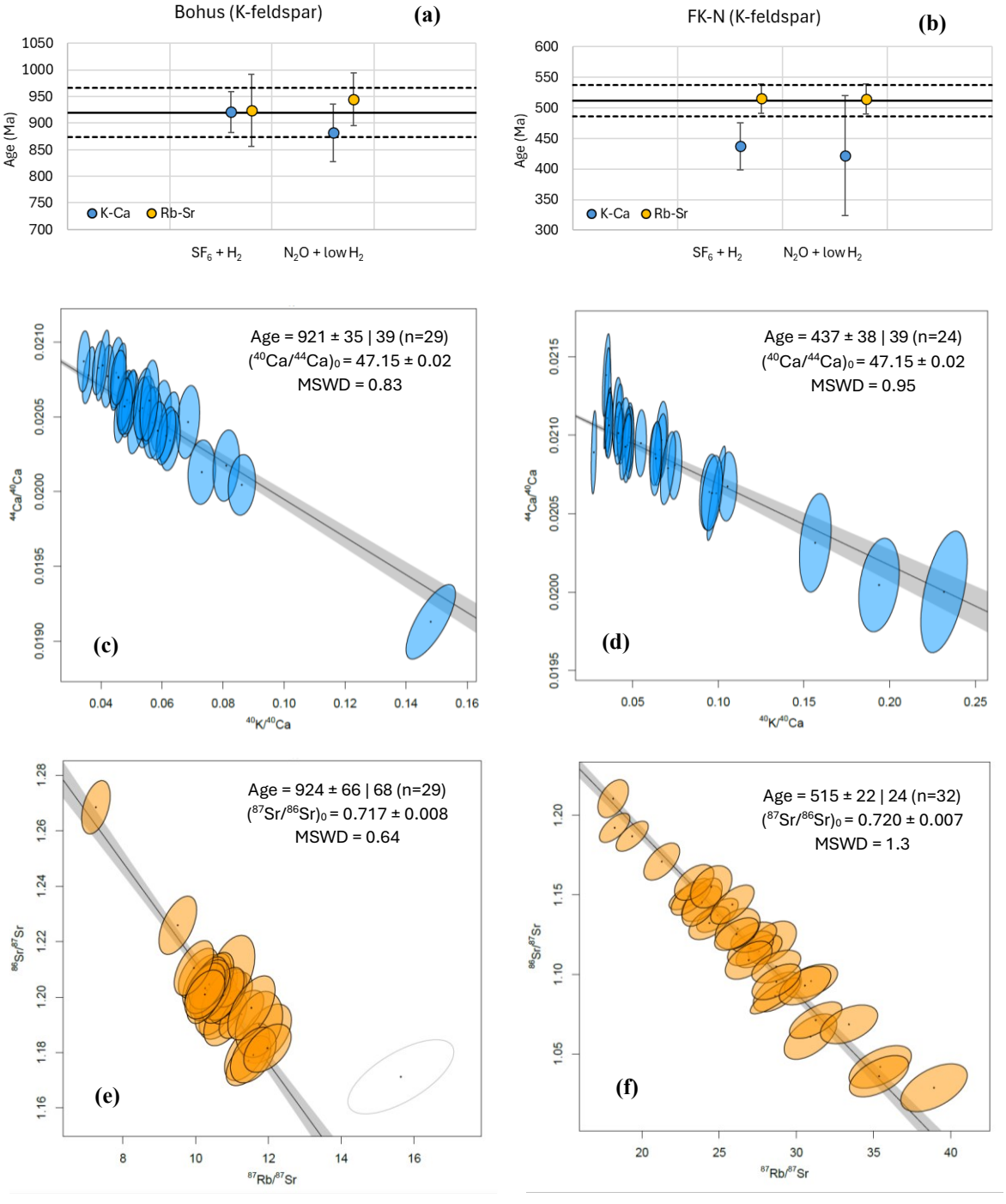

https://doi.org/10.5194/egusphere-2026-2790
Preprint. Discussion started: 2 June 2026

Figure 11. (a & b) Comparison in calculated K–Ca and Rb–Sr dates between the $SF_6 + H_2$ and N_2O + low H_2 reaction gas experiments for Bohus and FK-N feldspars. Uncertainty bars represent 2SE propagated uncertainties. Solid horizontal line represents expected age, dashed horizontal lines are ± 5% of expected age. Indicative K–Ca (c & d) and Rb–Sr (e & f) isochrons using $SF_6 + H_2$ reaction gas, with matrix matched age correction to MDC phlogopite. Analytical and total systematic age uncertainties are reported with the isochrons (x | y).

The Bohus and FK-N feldspars were analysed using $SF_6 + H_2$ and N_2O + low H_2 reaction gas mixtures (Fig. 11). The MDC corrected Rb–Sr and K–Ca dates are accurate within uncertainty for Bohus feldspar (921 ± 35 Ma and 924 ± 66 Ma, respectively using $SF_6 + H_2$), indicating no significant matrix bias between mica and felspars under the laser conditions used. In contrast, the K–Ca dates for FK-N were systematically younger than the Rb–Sr dates despite the large uncertainties (437 ± 38 Ma and 515 ± 22 Ma, respectively using $SF_6 + H_2$), indicating decoupling between the isotope systems. This younger K–Ca date could represent hydrothermal events recorded in the region (458–422 Ma, rutile U-Pb ages (Amal Dev and Tomson, 2024)) while the Rb-Sr date can be interpreted as a cooling age after the original emplacement of the granites during the late stages of the Pan African Orogeny (870–550 Ma, (Kröner and Stern, 2005)).

For both feldspars, the K–Ca date uncertainties are generally larger than the corresponding Rb–Sr date, due to the K–Ca system being less radiogenic (Fig. 11). Compared to the micas analysed, the feldspars are also significantly less radiogenic for both K–Ca and Rb–Sr. Multiple grains of FK-N and Bohus were mounted and tested for Ca concentration prior to analysis, and the lowest Ca grain was used for K-Ca measurements. These feldspars were selected due to their relatively low common Ca content (~ 300 ppm). Feldspars with higher Ca would be more challenging to analyse within 5% analytical precision on a quadrupole ICP-MS/MS, and a multi-collector-ICP-MS/MS may be advantageous for more precise $^{40}Ca/^{44}Ca$ measurements.

4.3 Current Limitations and Future Direction

The accuracy of the current technique is limited by the reference K–Ca age of the matrix matched reference material. In this study, we assume MDC has the same K–Ca age as reported for Rb–Sr. This proves to be valid in accurately reproducing the ages of Robins Folly and Högsbo muscovites within 2–3% uncertainty. However, independent validation of the K–Ca age would be required for the technique to develop further and to assess accuracy within 1–2% uncertainty, comparable to the in-situ Rb–Sr method. Recent work by (Olierook et al., 2026) has provided new Ar–Ar and Rb–Sr dates for a range of commonly used mica reference materials, and further characterisation of these micas for K–Ca would also be beneficial to the analytical community.

The low concentrations of common Ca, typical in micas, means the analyses can be easily compromised by Ca contamination. This can occur via remobilisation of previously ablated particulates in the interface tubing, especially after ablation of high Ca glasses such as NIST SRM 610 and BCR-2G, or from surface contamination during sample preparation and polishing. Using 5–10 shots of pre-ablation prior to the main analysis was found to minimise the impact of contamination, as well as cleaning the samples with distilled water in an ultra-sonic bath to remove particulates inside past ablation craters and/or crystal defects. The effects of contamination can be seen as spiky signals, especially for the minor ^{44}Ca, which leads to a young age bias in

https://doi.org/10.5194/egusphere-2026-2790
Preprint. Discussion started: 2 June 2026

contaminated data points (higher $^{44}Ca/^{40}Ca$ ratios). It may also, in part, explain the poor reproducibility of K–Ca dates between sessions (using the same reaction gas) for the highly radiogenic micas Kola and G17560 (< 5 ppm common Ca). Hence, sample cleaning and pre-ablation are paramount for accurate K–Ca dates.

There is also an upper limit of allowable Ca concentrations to resolve the amount of radiogenic ^{40}Ca ingrowth from the common Ca. For FK-N feldspar with ~ 300 ppm total K at ~ 500 Ma, the measured ^{40}Ca was 1–5 % radiogenic ($^{44}Ca/^{40}Ca$ = 0.02015-0.02099). Analysis using MC-ICP-MS/MS would improve the uncertainty on the $^{44}Ca/^{40}Ca$ ratio, enabling improved age precision and/or the ability to date younger Ca-bearing minerals such as feldspars. However, analysing both Rb–Sr and K–Ca simultaneously is currently only possible on a quadrupole ICP-MS/MS. An additional consideration is the pulse-analog transition of the EM detectors, which in this study was ~ 300 ppm total Ca.

One of the major advantages of quadrupole ICP-MS/MS is the ability to measure a wide range of isotopic masses in one analysis, hence simultaneous Rb–Sr, K–Ca and trace element analysis. However, when using SF_6 as the reaction gas, there are some limitations as to the additional trace element isotopes than can be measured due to isobaric interferences from reaction gas breakdown products. Specifically causing high backgrounds of: SF on ^{51}V, ^{52}Cr and ^{53}Cr, and SF_3 on ^{89}Y, ^{90}Zr and ^{91}Zr. As these interferences are created within the reaction cell, they cannot be avoided. Thus, care is needed for selection and interpretation of trace element data when using SF_6 as reaction gas.

5 Conclusions

This study directly compared SF_6 and N_2O combined with H_2 as reaction gasses for the simultaneous analysis of Rb–Sr and K–Ca isotope systems in micas and feldspars. Both Sr and Ca react efficiently to form either F or OH reaction products enabling analysis free from parent isotope isobaric interference (^{40}K and ^{87}Rb). The addition of H_2 is highly efficient in minimising the contribution from ^{40}Ar and reducing the backgrounds created from the high ion load in the reaction cell when targeting m/z 40. The gas combinations of SF_6 only, SF_6 plus H_2 or N_2O plus 7 ml min^{-1} H_2 were found to produce accurate data for micas within 2% and K-feldspars to within 5%. However, the combination of SF_6 plus H_2 gave the highest sensitivity and best signal to noise ratio. This is advantageous for achieving the best precision, especially for young micas or those with low common-Ca concentration.

We show that double dating of both K–Ca and Rb–Sr isotope systems is achievable from the same ablation volume for both mica and feldspars. This can be especially beneficial for small grains and/or detrital minerals where sample material is limited. Furthermore, in contrast to the initial $^{86}Sr/^{87}Sr$ ratio, the initial $^{44}Ca/^{40}Ca$ ratio is deemed invariable over geological timescales, thus single spot K–Ca dates can be determined from anchored 2-point isochrons (similar to Lu-Hf system), opening opportunities for detrital geochronology. Mineral dating via quadrupole LA-ICP-MS/MS is not only advantageous for simultaneous measurement of both isotope systems, it is also best suited for low Ca-bearing phases (5–300 ppm). Analysing this concentration range compliments TIMS and MC-ICP-MS/MS, which can achieve higher precision for high Sr & Ca bearing, low radiogenic phases.

https://doi.org/10.5194/egusphere-2026-2790
Preprint. Discussion started: 2 June 2026

The potential for decoupling between the isotope systems has been demonstrated with the FK-N feldspar from the Madras region, where the younger K–Ca date is likely to represent regional hydrothermal alteration, compared to the Rb–Sr date which has retained the crystallisation age of the granite. This newly developed technique, where isotope decoupling can be identified, will have wide usage for understanding cooling and alteration processes in micas and feldspars, and also increase knowledge of element diffusivity in these minerals.

Author Contributions

S. E Gilbert: Conceptualisation, data curation, methodology, formal analysis, investigation, validation, visualisation, writing – original, writing – review & editing.

S. Glorie: Conceptualisation, methodology, formal analysis, investigation, writing – review & editing.

J. Lloyd: Conceptualisation, methodology, visualisation, writing – review & editing

The authors declare that they have no conflict of interest.

Acknowledgements

We acknowledge and pay respects to the Kaurna People, the traditional custodians whose ancestral lands Adelaide University is built on and where the research was conducted. The authors would like to acknowledge the technical expertise of the fibre optics manufacturing team at the Institute for Photonics and Advanced Sensing, Adelaide University, especially to Dr. Mingze Yang for producing the reference material glasses. Also thank you to Thomas Zack and Delia Rösel for providing the Bohus and FK-N feldspar materials. Adelaide Microscopy, Adelaide University is a Microscopy Australia (ROR: 042mm0k03) facility enabled by NCRIS.

Financial support

This project was funded by an Australian Research Council Discovery Project: DP260104272.

Supplementary Material Tables

S1. Analytical Conditions

S2. K-Ca and Rb-Sr calculated dates

S3-8. Measured ratios and isochrons for all materials: (S3) SF_6 only; (S4 & 5) SF_6 + H_2; (S6 & 7) N_2O + 7 ml min^{-1} H_2; (S8) N_2O + 7 ml min^{-1} H_2

S9. Down hole fractionation curve Lambda values

https://doi.org/10.5194/egusphere-2026-2790
Preprint. Discussion started: 2 June 2026

References

Amal Dev, J. and Tomson, J. K.: U-Pb geochronology of rutiles from Southern granulite Terrane, India: Implications for the cooling and exhumation of East Gondwanan terranes, Precambrian Research, 407, doi:10.1016/j.precamres.2024.107408, 2024.

Amelin, Y. and Zaitsev, A. N.: Precise geochronology of phoscorites and carbonatites: The critical role of U-series disequilibrium in age interpretations, Geochimica et Cosmochimica Acta, 66, 2399–2419, 2002.

Antonelli, M. A. and Simon, J. I.: Calcium isotopes in high-temperature terrestrial processes, Chemical Geology, 548, doi: 10.1016/j.chemgeo.2020.119651, 2020.

Bayanova, T. B.: Baddeleyite: A Promising Geochronometer for Alkaline and Basic Magmatism, Petrology, 14, 187-200, 2006.

Brown, D. A., Simpson, A., Hand, M., Morrissey, L. J., Gilbert, S., Tamblyn, R., and Glorie, S.: Laser-ablation Lu-Hf dating reveals Laurentian garnet in subducted rocks from southern Australia, Geology, 50, 837-842, doi:10.1130/g49784.1, 2022.

Cherniak, D. J., Dimanov, A.: Diffusion in Pyroxene, Mica and Amphibole, Reviews in Mineralogy and Geochemistry, 72, 1, 641–690, doi:10.2138/rmg.2010.72.14, 2010

Craig, G., Wehrs, H., Bevan, D. G., Pfeifer, M., Lewis, J., Coath, C. D., Elliott, T., Huang, C., Lloyd, N. S., and Schwieters, J. B.: Project Vienna: A Novel Precell Mass Filter for Collision/Reaction Cell MC-ICPMS/MS, Anal Chem, 93, 10519-10527, doi:10.1021/acs.analchem.1c01475, 2021.

Dauphas, N., Hopp, T., Craig, G., Zhang, Z. J., Valdes, M. C., Heck, P. R., Charlier, B. L. A., Bell, E. A., Harrison, T. M., Davis, A. M., Dussubieux, L., Williams, P. R., Krawczynski, M. J., Bouman, C., Lloyd, N. S., Tollstrup, D., and Schwieters, J. B.: In situ 87Rb–87Sr analyses of terrestrial and extraterrestrial samples by LA-MC-ICP-MS/MS with double Wien filter and collision cell technologies, Journal of Analytical Atomic Spectrometry, 37, 2420-2441, doi:10.1039/d2ja00135g, 2022.

DePaolo, D. J.: Calcium Isotopic Variations Produced by Biological, Kinetic, Radiogenic and Nucleosynthetic Processes, Reviews in Mineralogy & Geochemistry, 55, 255-288, 2004.

Eiden, G. C., Barinaga, C. J., and Koppenaal, D. W.: Selective Removal of Plasma Matrix Ions in Plasma Source Mass Spectrometry, Journal of Analytical Atomic Spectrometry, 11, 317-322, 1996.

Eliasson, T. and Schöberg, H.: U-Pb dating of the post-kinematic Sveconorwegian (Grenvillian) Bohus granite, SW Sweden: evidence of restitic zircon, Precambrian Research, 51, 337-350, 1991.

Farkaš, J.: Calcium Isotopes, in: Encyclopedia of Geochemistry, Encyclopedia of Earth Sciences Series, 1-6, doi:10.1007/978-3-319-39193-9_237-1, 2016.

Fletcher, I. R., McNaughton, N. J., Pidgeon, R. T., and Rosman, K. J. R.: Sequential closure of K–Ca and Rb–Sr isotopic systems in Archaean micas, Chemical Geology, 138, 289-301, 1997.

https://doi.org/10.5194/egusphere-2026-2790
Preprint. Discussion started: 2 June 2026

Gilbert, S. E., Glorie, S., and Zack, T.: In situ beta decay dating by LA-ICP-MS/MS: applications, in: Methods and Applications of Geochronology, Elsevier, 243-295, 2024.

Gilbert, S. E., Danyushevsky, L. V., Rodemann, T., Shimizu, N., Gurenko, A., Meffre, S., Thomas, H., Large, R. R., and Death, D.: Optimisation of laser parameters for the analysis of sulphur isotopes in sulphide minerals by laser ablation ICP-MS, J. Anal. At. Spectrom., 29, doi:1042-1051, 10.1039/c4ja00011k, 2014.

Giletti, B. J.: Rb and Sr diffusion in alkali feldspars, with implications for cooling histories of rocks, Geochimica et Cosmochimica Acta, 55, 5, 1331–1343, doi:10.1016/0016-7037(91)90311-R, 1991

Glorie, S., Gilbert, S. E., Hand, M., and Lloyd, J. C.: Calibration methods for laser ablation Rb–Sr geochronology: comparisons and recommendation based on NIST glass and natural reference materials, Geochronology, 6, 21-36, doi:10.5194/gchron-6-21-2024, 2024a.

Glorie, S., Simpson, A., Gilbert, S. E., Hand, M., and Müller, A. B.: Testing the reproducibility of in situ LuHf dating using Lu-rich garnet from the Tørdal pegmatites, southern Norway, Chemical Geology, 653, 122038, doi:10.1016/j.chemgeo.2024.122038, 2024b.

Glorie, S., Mulder, J., Hand, M., Fabris, A., Simpson, A., and Gilbert, S.: Laser ablation (in situ) Lu-Hf dating of magmatic fluorite and hydrothermal fluorite-bearing veins, Geoscience Frontiers, 14, 6, 101629, 2023.

Gopalan, K.: Conjunctive K–Ca and Rb–Sr dating of glauconites, Chemical Geology, 247, 119-123, doi:10.1016/j.chemgeo.2007.10.004, 2008.

Gorojovsky, L. and Alard, O.: Optimisation of laser and mass spectrometer parameters for the in situ analysis of Rb/Sr ratios by LA-ICP-MS/MS, Journal of Analytical Atomic Spectrometry, 35, 2322-2336, doi:10.1039/d0ja00308e, 2020.

Govindaraju, K.: Report (1968-1978) on Two Mica Reference Samples: Biotite Mica-Fe and Phlogopite Mica-Mg, Geostandards Newsletter, 3, 3-24, 1979.

Govindaraju, K.: Report (1973 - 1984) on Two ANRT Geochemical Reference Samples: Granite GS-N and Potash Feldspar FK - N, Geostandards Newsletter, 8, 173-206, 1984.

Govindaraju, K.: Working values with confidence limits for twenty-six CRPG, ANRT and IWG-GIT geostandards, Geostandards Newsletter, 19, 1-32, 1995.

Hammouda, T., Cherniak, D. J.: Diffusion of Sr in fluorphlogopite determined by Rutherford backscattering spectrometry, Earth and Planetary Science Letters, 178, 3, 339–349, doi:10.1016/S0012-821X(00)00089-3, 2000

Harrison, T. M. and Lovera, O. M.: The multi-diffusion domain model: Past, present and future, in: Advances in 40Ar/39Ar Dating: From Archaeology to Planetary Sciences., edited by: Jourdan, F., Mark, D. F., and Verati, C., Geological Society, London, pp. 91-106, 2014.

Heuser, A., Eisenhauer, A., Gussone, N., Bock, B., Hansen, B. T., and Hagler, T. F.: Measurement of calcium isotopes (δ44Ca) using a multicollector TIMS technique, International Journal of Mass Spectrometry, 220, 385-397, 2002.

https://doi.org/10.5194/egusphere-2026-2790
Preprint. Discussion started: 2 June 2026

Hogmalm, K. J., Dahlgren, I., Fridolfsson, I., and Zack, T.: First in situ Re-Os dating of molybdenite by LA-ICP-MS/MS, Mineralium Deposita, 54, 821-828, doi:10.1007/s00126-019-00889-1, 2019.

Hogmalm, K. J., Zack, T., Karlsson, A. K. O., Sjöqvist, A. S. L., and Garbe-Schönberg, D.: In situ Rb–Sr and K–Ca dating by LA-ICP-MS/MS: an evaluation of N2O and SF6 as reaction gases, Journal of Analytical Atomic Spectrometry, 32, 305-313, doi:10.1039/c6ja00362a, 2017.

Jackson, S. E.: Calibration strategies for elemental analysis by LA-ICP-MS., in: Mineralogical Association of Canada Short Course, Vancouver, 169-188, 2008.

Jegal, Y., Zimmermann, C., Reisberg, L., Yeghicheyan, D., Cloquet, C., Peiffert, C., Gerardin, M., Deloule, E., and Mercadier, J.: Characterisation of Reference Materials for in-situ Rb-Sr dating by LA-ICP-MS/MS, Geostandards and Geoanalytical Research, 645-671, doi:10.1111/ggr.12456, 2022.

Jenkin, G. R. T.: Do cooling paths derived from mica Rb-Sr data reflect true cooling paths?, Geology, 25, 907, doi:10.1130/0091-7613(1997)025<0907:dcpdfm>2.3.co;2, 1997.

Krasnova, N. y.: The Kovdor phlogopite deposit, Kola Peninsula, Russia, The Canadian Mineralogist, 39, 33-44, 2001.

Kröner, A. and Stern, R. J.: Pan-African Orogeny, in: Encyclopaedia of Geology, edited by: Selley, R. C., Cocks, L. R. M., and Plimer, I. R., Elsevier, 1-12, 2005.

Laureijs, C. T., Coogan, L. A., and Spence, J.: In-situ Rb-Sr dating of celadonite from altered upper oceanic crust using laser ablation ICP-MS/MS, Chemical Geology, 579, 120339, doi:10.1016/j.chemgeo.2021.120339, 2021a.

Laureijs, C. T., Coogan, L. A., and Spence, J.: Regionally variable timing and duration of celadonite formation in the Troodos lavas (Cyprus) from Rb-Sr age distributions, Chemical Geology, 560, 119995, doi:10.1016/j.chemgeo.2020.119995, 2021b.

Li, S.-S., Santosh, M., Farkaš, J., Redaa, A., Ganguly, S., Kim, S. W., Zhang, C., Gilbert, S., and Zack, T.: Coupled U-Pb and Rb-Sr laser ablation geochronology trace Archean to Proterozoic crustal evolution in the Dharwar Craton, India, Precambrian Research, 343, 105709, doi:10.1016/j.precamres.2020.105709, 2020.

Li, Y. and Vermeesch, P.: Short communication: Inverse isochron regression for Re–Os, K–Ca and other chronometers, Geochronology, 3, 415-420, 2021.

Liebmann, J., Kirkland, C. L., Kelsey, D. E., Korhonen, F. J., and Rankenburg, K.: Lithological fabric as a proxy for Rb–Sr isotopic complexity, Chemical Geology, 608, doi:10.1016/j.chemgeo.2022.121041, 2022.

Lloyd, J. C., Spandler, C., Gilbert, S. E., and Hasterok, D.: The quantification of downhole fractionation for laser ablation mass spectrometry, EGUsphere, 1-28, 2024.

Loyola, C., Farkaš, J., Collins, A. S., Gilbert, S. E., Verdel, C., Löhr, S. C., Brock, G. A., Shields, G. A., Baldermann, A., Redaa, A., Blades, M., Subarkah, D., Bishop, C., Giles, S. M., Christie-Blick, N., and Haines, P. W.: In situ Rb–Sr dating and REE analysis of glauconites and detrital feldspars from the Ediacaran/Cambrian strata: Centralian and Adelaide Superbasins, Australia, Precambrian Research, 427, 10.1016/j.precamres.2025.107851, 2025.

https://doi.org/10.5194/egusphere-2026-2790
Preprint. Discussion started: 2 June 2026

Marshall, B. D.: Potassium-calcium decay system, in: Geochemistry. Encyclopaedia of Earth Science, Springer, Dordrecht, doi.org/10.1007/1-4020-4496-8_260, 1998.

Morteani, G., Kostitsyn, Y. A., Gilg, H. A., Preinfalk, C., and Razakamanana, T.: Geochemistry of phlogopite, diopside, calcite, anhydrite and apatite pegmatites and syenites of southern Madagascar: evidence for crustal silicocarbonatitic (CSC) melt formation in a Panafrican collisional tectonic setting, International Journal of Earth Sciences, 102, 627-645, doi:10.1007/s00531-012-0832-x, 2013.

Mortimer, G. E., Cooper, J. A., and James, P. R.: U-Pb and Rb-Sr geochronology and geological evolution of the Harts Range ruby mine area of the Arunta Inlier, central Australia, Lithos, 20, 445-467, 1987.

Nägler, T. F., Villa, I. M.:In pursuit of the 40K branching ratios: K-Ca and 39Ar-40Ar dating of gem silicates, Chemical Geology, 169, 1-2, 5-16, doi.org/10.1016/S0009-2541(99)00194-1, 2000.

Nebel, O.: Rb–Sr Dating, Encyclopedia of Scientific Dating Methods, Springer Science+Business Media, 1-19, doi:10.1007/978-94-007-6326-5_116-1, 2014.

Norris, A. and Danyushevsky, L.: Towards Estimating the Complete Uncertainty Budget of Quantified Results Measured by LA-ICP-MS, Goldschmidt, Boston, 2018.

Olierook, H. K. H., Rankenburg, K., Ulrich, S., Kirkland, C. L., Evans, N. J., Brown, S., McInnes, B. I. A., Prent, A., Gillespie, J., McDonald, B., and Darragh, M.: Resolving multiple geological events using in situ Rb–Sr geochronology: implications for metallogenesis at Tropicana, Western Australia, Geochronology, 2, 283-303, doi:10.5194/gchron-2-283-2020, 2020.

Olierook, H. K. H., Ribeiro, B. V., Liebmann, J., Rankenburg, K., Jourdan, F., Redaa, A., Lloyd, J. C., Belgrano, T. M., Corella Santa Cruz, C. R., Jegal, Y., Mercadier, J., Yu, J., Zametzer, A., Kirkland, C. L., Rohrer, R., Storey, C., Doucet, L. S., Jones, I., Stokes, L., Zack, T., Rösel, D., Hébert, N., Fougerouse, D., Kaempf, J., Datta, P., Hameed, H., Evans, N. J., Roberts, M., Mayers, C., Frew, A., Al Odeh, S., Roche, C. E., Chiaradia, M., Cruz-Uribe, A. M., Collins, A. S., Gilbert, S. E., Farkaš, J., Glorie, S., Karlsson, A., and Kumara, A. S.: Appraisal of eight natural mica reference materials for in situ Rb-Sr geochronology, Geostandards and Geoanalyical Research, in press, 2026.

Pandey, B., Krishna, V., Sastry, D., Chabria, T., Mary, K., and Dhanaraju, R.: Pan-African wholerock Rb–Sr isochron ages for the granites and pegmatites of Kullampatti–Suriyamalai area, Salem District, Tamil Nadu, India, Mass Spectrometry'IIP, Dehra Dun, 1993.

Pedrosa-Soares, A. C., De Campos, C. P., Noce, C., Silva, L. C., Novo, T., Roncato, J., Medeiros, S., Castañeda, C., Queiroga, G., Dantas, E., Dussin, I., and Alkmim, F.: Late Neoproterozoic-Cambrian granitic magmatism in the Araçuaí orogen (Brazil), the Eastern Brazilian Pegmatite Province and related mineral resources, Geological Society, London, Special Publications, 350, 25-51, doi:10.1144/sp350.3, 2011.

Redaa, A., Farkaš, J., Gilbert, S., Collins, A. S., Wade, B., Löhr, S., Zack, T., and Garbe-Schönberg, D.: Assessment of elemental fractionation and matrix effects during in situ Rb–Sr dating of phlogopite by LA-ICP-MS/MS: implications

https://doi.org/10.5194/egusphere-2026-2790
Preprint. Discussion started: 2 June 2026

for the accuracy and precision of mineral ages, Journal of Analytical Atomic Spectrometry, 36, 322-344, doi:10.1039/d0ja00299b, 2021.

Redaa, A., Farkaš, J., Gilbert, S., Collins, A. S., Löhr, S., Vasegh, D., Forster, M., Blades, M., Zack, T., Giuliani, A., Maas, R., Baldermann, A., Dietzel, M., and Garbe-Schönberg, D.: Testing Nano-Powder and Fused-Glass Mineral Reference Materials for In Situ Rb-Sr Dating of Glauconite, Phlogopite, Biotite and Feldspar via LA-ICP-MS/MS, Geostandards and Geoanalytical Research, 47, 23-48, doi:10.1111/ggr.12467, 2022.

Renne, P. R., Balco, G., Ludwig, K. R., Mundil, R., and Min, K.: Response to the comment by W.H. Schwarz et al. on "Joint determination of 40K decay constants and 40Ar*/ 40K for the Fish Canyon sanidine standard, and improved accuracy for 40Ar/39Ar geochronology" by P.R. Renne et al. (2010), Geochimica et Cosmochimica Acta, 75, 5097-5100, 2011.

Rieder, M., Cavazzini, G., D'yakonov, Y.S., Frank-Kamenetskii, V.A., Gottardi, G., Guggenheim, S., Koval, P. W., Müller, G. Neiva, A. M. R., Radoslovich, E. W., Robert, J-L., Sassi, F. P., Takeda, H., Weiss, Z., Wones, D. R.: Nomenclature of the Micas, Clays and Clay Minerals, 46, 5, 586–595, doi:10.1346/CCMN.1998.0460513, 1998

Romer, R. L. and Smeds, S.-A.: U-Pb columbite ages of pegmatites from Sveconorwegian terranes in southwestern Sweden, Precambrian Research, 76, 15-30, 1996.

Rösel, D. and Zack, T.: LA-ICP-MS/MS Single-Spot Rb-Sr Dating, Geostandards and Geoanalytical Research, doi:10.1111/ggr.12414, 2022.

Russell, W. A., Papanastassiou, D. A., and Tombrella, T. A.: Ca isotope fractionation on the Earth and other solar system materials, Geochimica et Cosmochimica Acta, 42, 1075-1090, 1978.

Simpson, A., Glorie, S., Hand, M., Spandler, C., and Gilbert, S.: Garnet Lu-Hf speed dating: A novel method to rapidly resolve polymetamorphic histories, Gondwana Research, 121, 215–234, https://doi.org/10.1016/j.gr.2023.04.011, 2023.

Simpson, A., Gilbert, S., Tamblyn, R., Hand, M., Spandler, C., Gillespie, J., Nixon, A., and Glorie, S.: In-situ Lu Hf geochronology of garnet, apatite and xenotime by LA ICP MS/MS, Chemical Geology, 577, 120299, doi:10.1016/j.chemgeo.2021.120299, 2021.

Skiöld, T.: The interpretation of the Rb-Sr and K-Ar ages of late Precambrian rocks in south-western Sweden, Geologiska Föreningen i Stockholm Förhandlingar, 98, 3-29, https://doi.org/10.1080/11035897609454335, 2010.

Subarkah, D., Nixon, A. L., Jimenez, M., Collins, A. S., Blades, M. L., Farkaš, J., Gilbert, S. E., Holford, S., and Jarrett, A.: Constraining the geothermal parameters of in situ Rb–Sr dating on Proterozoic shales and their subsequent applications, Geochronology, 4, 577-600, doi:10.5194/gchron-4-577-2022, 2022.

Tamblyn, R., Hand, M., Simpson, A., Gilbert, S., Wade, B., and Glorie, S.: In situ laser ablation Lu–Hf geochronology of garnet across the Western Gneiss Region: campaign-style dating of metamorphism, Journal of the Geological Society, 179, doi:10.1144/jgs2021-094, 2022.

Tamblyn, R., Gilbert, S., Glorie, S., Spandler, C., Simpson, A., Hand, M., Hasterok, D., Ware, B., and Tessalina, S.: Molybdenite Reference Materials for In Situ LA-ICP-MS/MS Re-Os Geochronology, Geostandards and Geoanalytical Research, 48, 393-410, 2024.

https://doi.org/10.5194/egusphere-2026-2790
Preprint. Discussion started: 2 June 2026

Tillberg, M., Drake, H., Zack, T., Hogmalm, J., Kooijman, E., and Åström, M.: Reconstructing craton-scale tectonic events via in situ Rb-Sr geochronology of poly-phased vein mineralization, Terra Nova, 33, 502-510, doi:10.1111/ter.12542, 2021.

Tillberg, M., Drake, H., Zack, T., Kooijman, E., Whitehouse, M. J., and Astrom, M. E.: In situ Rb-Sr dating of slickenfibres in deep crystalline basement faults, Sci Rep, 10, 562, doi:10.1038/s41598-019-57262-5, 2020.

Tischendorf, G., Förster, H.-J., Gottesmann, B., and Rieder, M.: True and brittle micas: composition and solid-solution series, Mineralogical Magazine, 71, 285-320, 2007.

Villa, I. M., De Bièvre, P., Holden, N. E., and Renne, P. R.: IUPAC-IUGS recommendation on the half life of 87Rb, Geochimica et Cosmochimica Acta, 164, 382-385, https://doi.org/10.1016/j.gca.2015.05.025, 2015.

Wang, C., Alard, O., Lai, Y.-J., Foley, S. F., Liu, Y., Munnikhuis, J., and Wang, Y.: Advances in in-situ Rb-Sr dating using LA-ICP-MS/MS: applications to igneous rocks of all ages and to the identification of unrecognized metamorphic events, Chemical Geology, 610, doi:10.1016/j.chemgeo.2022.121073, 2022.

Zack, T. and Gilbert, S. E.: In situ beta decay dating by LA-ICP-MS/MS: Fundamentals and methodology, in: Methods and Applications of Geochronology, Elsevier, 211-241, 2024.

Zack, T. and Hogmalm, K. J.: Laser ablation Rb/Sr dating by online chemical separation of Rb and Sr in an oxygen-filled reaction cell, Chemical Geology, 437, 120-133, doi:10.1016/j.chemgeo.2016.05.027, 2016.

Zhao, J., Chen, H., Xiao, B., Zhu, Y., and Wang, H.: Substitution mechanism controls on compositional variations and spectral responses of white micas in major hydrothermal systems, Applied Clay Science, 269, 107762, 2025.